https://doi.org/10.1142/9789811280184_0023

Chapter 23

Electron-Hadron Scattering resolving Parton Dynamics

Néstor Armesto

Instituto Galego de Física de Altas Enerxías IGFAE, Universidade de Santiago de Compostela, 15782 Santiago de Compostela, Galicia-Spain

Claire Gwenlan

Department of Physics, University of Oxford, Denys Wilkinson Building, Keble Road, Oxford. OX1 3RH. United Kingdom

Anna Stasto

Department of Physics, The Pennsylvania State University University Park, PA 16802, U.S.A.

1. Resolving the Dynamics of Partons in Protons and Nuclei

The LHeC opens a new kinematic realm in the study of the structure of protons and nuclei through their scattering with leptons — electrons or positrons. As illustrated in Fig. 1(left), in *ep* it extends the region of the $x - Q^2$ kinematic plane studied at HERA by one order of magnitude up in Q^2 and down in Bjorken x, $Q^2 = 1 - 10^6$ GeV and $x = 10^{-6} - 0.9$.[a] The expected *ep* integrated luminosity, 1 ab^{-1}, exceeds that at HERA by three orders of magnitude. In electron-nucleus collisions, Fig. 1(right), the expected increase is three to four orders of magnitude down in x and up in Q^2 compared to previous DIS experiments, with an anticipated per

[a]The Electron-Ion Collider (EIC) will explore a more restricted kinematic region than HERA, but its high luminosity, the new detector techniques, and the possibility to accelerate polarised protons and vary the nuclear species, will provide valuable information on the three-dimensional structure of hadrons and nuclei and on the origin of spin.[3]

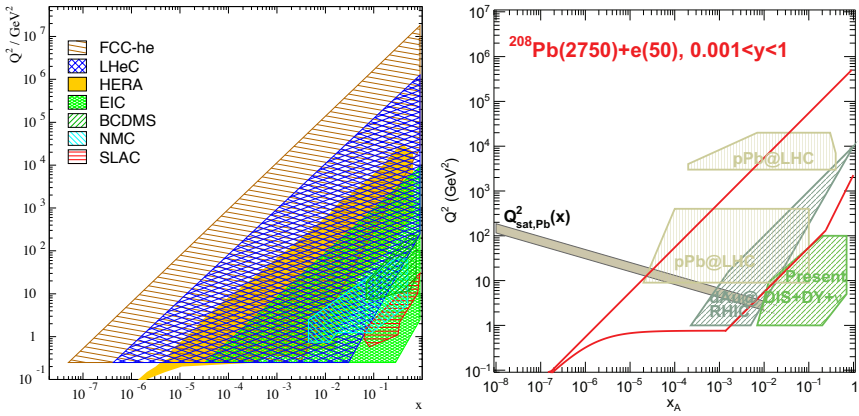

Fig. 1. Kinematic plane for ep (left) and ePb (right) collisions at the LHeC,[1] compared with the coverage of past and projected accelerators. Figures taken from Refs. 1,2, where further details can be found.

nucleon integrated luminosity ~ 10 fb^{-1}. Such features, together with the clean final state allowing a complete reconstruction of kinematic variables, as well as current and projected detector and theoretical developments, guarantee that the LHeC will result in a leap in our understanding of the partonic structure of protons and nuclei. Here, we briefly develop some of the possibilities studied in Ref. 1.

1.1. *Proton parton densities in lepton-proton collisions*

The LHeC offers the single opportunity to pin down, with high precision, the partonic structure of the proton, over an unprecedented kinematic range of DIS (see Fig. 1(left)). Through a combination of precision measurements of charged current (CC) and neutral current (NC) DIS spanning, respectively, four and six orders of magnitude in (x, Q^2), supplemented by semi-inclusive measurements of strange and heavy flavour quark production, all parton distribution functions (PDFs) $xq(x, Q^2)$ and $xg(x, Q^2)$ can be separately determined in a single experiment.[b] The EIC[3] can also provide such information, but primarily in the much reduced kinematic range previously covered by HERA and fixed target experiments. The large centre-of-mass energy of the LHeC, and its higher energy version, the FCC-eh, is therefore essential to probe the full kinematic range of relevance for the HL-LHC, and later the FCC, and allows unique access to the unexplored small-x regime, as discussed in Sec. 3.

[b] $q = u_v, d_v, u, \bar{u}, d, \bar{d}, s, c, b$ as well as t.

Maximum exploitation of the HL-LHC physics era would be made possible by an accompanying LHeC precision QCD programme. The delivery of the full complement of parton densities to unprecedented precision, together with α_s to per mille accuracy, derived from measurements that are experimentally and theoretically clean, and independent of the pp environment, would establish a new paradigm for understanding perturbative QCD and the underlying parton dynamics. Furthermore, it would enable extraordinarily precise electroweak and Higgs physics at the joint ep and pp LHC facility, and extend and facilitate the prospects for new physics discovery and interpretation.

The projected precision of the valence quark (xu_v, xd_v), anti-sea quark ($x\overline{U}$, $x\overline{D}$) and gluon (xg) densities, from LHeC inclusive NC and CC measurements, defined through a standard $\Delta\chi^2 = 1$ applicable for a single experiment with consistent measurements, is illustrated in Fig. 2. Ideally, LHeC data would be available at the same time as HL-LHC operation; therefore, two projections are shown: one corresponding to an initial dataset of 50 fb^{-1} (yellow), and the other to the full 1 ab^{-1} of inclusive DIS data (dark blue). The LHeC projections are compared to HERAPDF2.0[4] (light blue) and several other modern global fits.[5–8] Notably, in addition to large uncertainties on individual sets, especially at small and large x, where current data is scarce or suffers from large uncertainties, an unsatisfactory situation is evident, whereby differences between global fits can be larger than the quoted uncertainties. This arises from a combination of factors, including those related to underlying assumptions in the fits, as well as the complexity of hadron-hadron scattering data, as used in the global fits, with respect to DIS. These include issues related to initial state quark radiation, hadronisation, complex experimental uncertainty correlations, and potentially incompatible datasets, which can lead to inflation of uncertainties and/or exclusion of certain datasets. In contrast, DIS processes have clean final states and (with a precedent set by HERA) experimentally precise, compatible sets of measurements, with well understood systematic uncertainties and correlations, can be achieved, supplemented by sophisticated theoretical calculations.

1.1.1. *Valence and light sea quarks*

The valence quark and light sea antiquark distributions are shown in Fig. 2 top and middle. The projection for the LHeC initial run, which corresponds to a two orders of magnitude increase in integrated luminosity compared

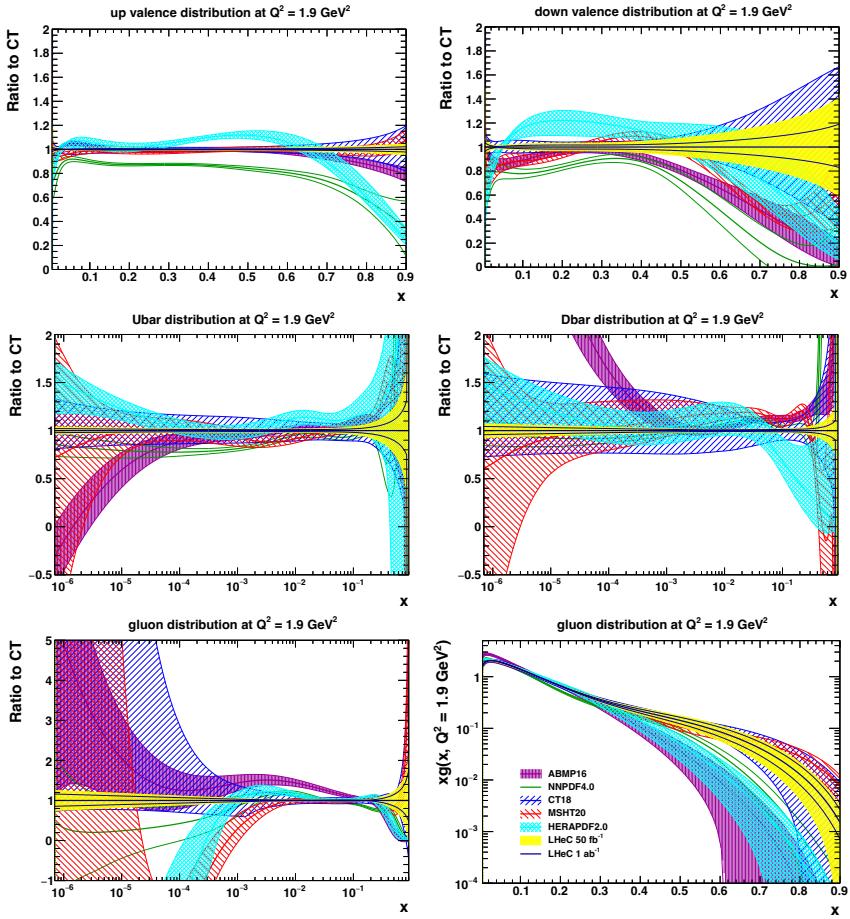

Fig. 2. Expected precision for the determination of the u_v and d_v (top), $\overline{U} = \bar{u}$ and $\overline{D} = \bar{d} + \bar{s}$ (middle), and gluon (bottom) PDFs from the LHeC. The gluon distribution is shown as a ratio on a log-x scale (left) and as the full distribution on a linear-x scale (right) to highlight both the small- and large-x regions. Light blue: HERA, yellow: initial LHeC run, dark blue: full inclusive LHeC dataset, overlayed with four recent global fit results. For more information, see Ref. 1.

to that collected by the general purpose HERA experiments, shows a striking improvement in uncertainties across the full range of Bjorken-x, compared to today.[c] The 1 ab^{-1} projection, which mainly includes e^-p but

[c]Note that, following convention, while the parton distributions are shown at the starting scale of the QCD fit, $Q^2 = 1.9$ GeV^2, the improvements illustrated are representative, and persist from low to high scales.

also 1 fb^{-1} of e^+p simulated collision data, provides additional constraints, most notably at the highest x values. This arises primarily from the larger integrated luminosity, which allows precise NC and CC measurements at the highest (x, Q^2) values. Additionally, in the valence sector, the small amount of positron data gives access to u_v and d_v at small x from the $e^{\pm}p$ cross section differences, as well as additional sensitivity to d_v at high x, via the CC process. The expected precision on the valence quark distributions has strong implications for new physics searches at the HL-LHC, as well as in resolving the long-standing mystery of the unknown d/u ratio at large x. The light (anti)quark sea distributions are currently rather poorly known, especially at small and large x. In the smaller x region, the sea quark distributions are large and play a significant role in precision standard model measurements at hadron colliders, while at high x the distributions are small, but important for searches at high mass, for which the sea and valence components must be properly distinguished. The LHeC would provide a transformation in precision (Fig. 2(middle)) as a result of the precise NC and CC measurements that probe down to the small-x regime while at high Q^2. In particular, the combination of CC cross sections (which can be well measured for $x \gtrsim 10^{-4}$), together with NC (which has both electromagnetic and weak contributions with different dependencies on flavour composition), can distinguish between u- and d-type sea (anti)quarks. This was not possible at HERA due to the limited precision at high Q^2. Moreover, it is worth noting that this is a unique feature of a high energy ep collider. For example, at the EIC, assuming a detection threshold of $Q^2 \approx 100$ GeV^2, the CC cross section will be precisely measurable only in the region above $x \approx 10^{-2}$ (see Fig. 1(left)), and so quark flavour can be disentangled only above this value.

1.1.2. *Strange and heavy flavour quarks*

The strange content of the proton is still poorly known, and has historically been the subject of some controversy,[9–20] yet it is highly relevant for standard model precision measurements at hadron colliders including, for instance, the W mass. At the LHeC, the strange density $xs(x, Q^2)$ can be precisely mapped, for the first time, via charm tagging in the $Ws \to c$ process, in CC events. Furthermore, the LHeC provides data on charm and beauty quarks from measurements of the structure functions F_2^c and F_2^b, extending over nearly five or six orders of magnitude, even with just a subset of the full integrated luminosity.[1] Such measurements not only serve

to directly determine xc and xb, and provide information on the correct theoretical treatment for heavy quarks, but also provide additional constraints on the gluon parton density, xg, and can be used to improve the determinations of the charm and beauty masses, bringing uncertainties to $\delta m_{c(b)} \simeq 3(10)$ MeV.[1] Furthermore, due to the large centre-of-mass energy and integrated luminosity, the LHeC opens up the possibility of studying top quark PDFs as a new avenue of research.

1.1.3. *Gluon and α_s*

Precise knowledge of the gluon PDF across the full range of x is of fundamental importance, and can be profoundly addressed at the LHeC. In principle, the projected improvements, see Fig. 2(bottom), are due to the large kinematic range and precise measurements of scaling violations,

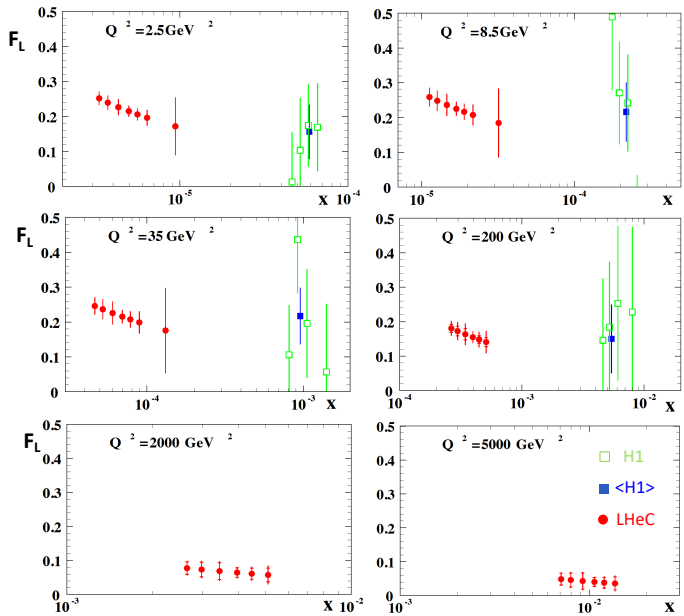

Fig. 3. H1 measurement[21] (green and blue) and LHeC projection for $F_L(x, Q^2)$ (red), derived from simulated inclusive cross section data with $E_p = 7$ TeV and $E_e = 60$, 30, 20 GeV. The LHeC inner error bars represent the statistical uncertainty, only visible for $Q^2 \geqslant 200$ GeV^2, and the outer error bars show the total uncertainty. The LHeC simulated data cover an x-range from 2×10^{-6} to above $x = 0.01$. Full details given in Ref. 1.

$\partial F_2/\partial \ln Q^2$, as well as the fact that the inclusive NC and CC measurements, together, provide a base to fully constrain the quark distributions which, in turn, strongly constrain xg. The LHeC extends to smaller x than HERA by more than an order of magnitude, allowing unique access to the small-x region. The addition of a precise measurement of the longitudinal structure function, F_L, achievable at the LHeC using dedicated low energy runs, as illustrated in Fig. 3,[1] would unravel the non-linear behaviour of xg at small x (see also Sec. 3). Not only would this lead to a revolution in understanding the underlying parton dynamics, it also has particular significance for both signal and background in precision physics at the HL-LHC, and even more so for the FCC where, for instance, Higgs becomes small-x physics, and the gluon must be accurately known, given the dominant $gg \to H$ production mechanism. The large-x gluon, which has significance for searches at high masses, is also constrained, primarily via the momentum sum rule as a result of the precise determination of valence and sea quarks at high x. Importantly, further direct constraints on xg can come from measurements of jet cross sections and $F_2^{c,b}$, as well as F_L for the small-x region, none of which are included in the studies represented in Fig. 1. Finally, a simultaneous QCD analysis for parton distributions and the strong coupling α_s, using inclusive NC and CC together with DIS inclusive jet measurements, results in projected α_s uncertainties at the per mille level.

1.2. *Inclusive scattering and parton densities in electron-nucleus collisions*

Lepton-nucleus collisions at the LHeC will allow the precise extraction of the partonic nuclear structure in a completely new kinematic region, see Fig. 1(right). The EIC[3] will provide such information but only in the region covered by fixed target and dAu data, and limited by kinematics, e.g., by the lack of access to CC at small x to determine the strangeness content of nucleons inside nuclei. Higher centre-of-mass energies are required to study the region relevant for nuclear collisions at the LHC and future hadronic colliders, with DIS providing a complete reconstruction of kinematic variables and a cleaner theoretical environment compared to proton-nucleus collisions.

While the expected integrated luminosity is considerably smaller than in ep, even with 1 fb^{-1} a complete unfolding of the different flavours for a single nucleus will still be possible for $x \gtrsim 10^{-5}$, using the same combination of inclusive observables employed in ep.[1] The resulting uncertainties

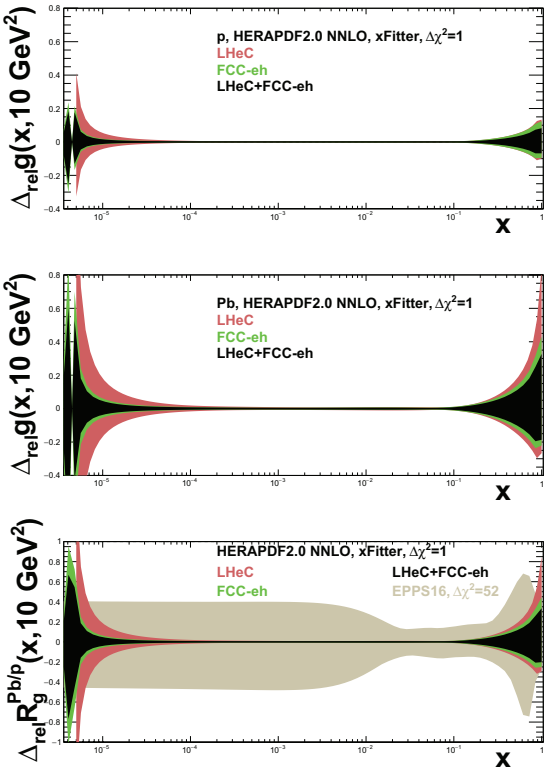

Fig. 4. Relative uncertainty of the gluon density in the proton (top), Pb (middle) and the corresponding nuclear modifications factor (bottom) in an analysis of ep and ePb LHeC and FCC-eh NC plus CC pseudodata using *xFitter* (both a single set of data and all combined), compared to the results of EPPS16.[22] Taken from Ref. 1.

(see Fig. 4), defined through a standard $\Delta\chi^2 = 1$ applicable for a single experiment, will be much smaller than the ones in global fits that employ a much larger tolerance and that, due to the scarcity of data for a single nuclear species, require initial conditions that depend on the nuclear size.

The determination with small uncertainties of parton densities for the different species both in ep and eA will clarify how the partonic structure of a nucleon is affected by the nuclear medium,[1] in different kinematic regions: the origin of shadowing at small x and its eventual relation to diffraction (see below), the dependence of antishadowing on the parton flavour, the Q^2 evolution of the EMC effect, the nuclear dependence of intrinsic charm etc.

Finally, let us note that the lack of knowledge of nuclear PDFs is among the largest sources of uncertainty in the extraction of properties of the medium produced in heavy ion collisions, the quark gluon plasma. Also note that factorisation is assumed in such studies. Therefore, they will be greatly benefited by the precise knowledge of PDFs obtained in DIS which will also allow precise tests of factorisation in proton-nucleus collisions.

2. Diffractive scattering and three dimensional structure

In the DIS diffractive event $e + p \to p(Y) + X$ the incoming proton p is scattered elastically or dissociates into a small mass excitation Y, while being well separated by a *rapidity gap* from the diffractive system X, see Fig. 5. The rapidity gap is a region in the detector completely devoid of any activity. The mechanism responsible for creating rapidity gaps must involve a colour singlet exchange, so that no QCD radiation can be produced into this region.

The precise measurement of diffraction in electron-hadron collisions is of great importance for our understanding of the dynamics of the strong interaction. Since diffraction is mediated by colour neutral exchange, the exact mechanism governing this exchange can provide information about confinement. Also, an important contribution to the diffractive exchange

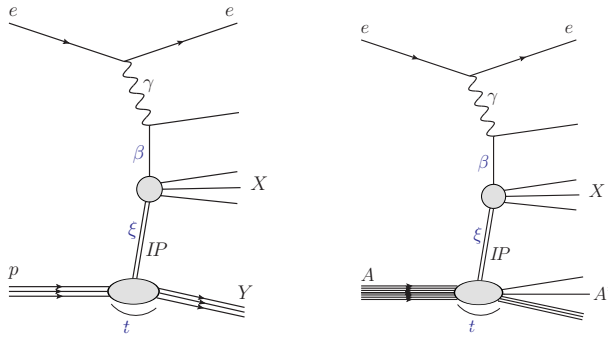

Fig. 5. Left: diffractive process in DIS. Y is either the elastically scattered proton or a low mass excitation, IP is the colour singlet exchange ('Pomeron') responsible for rapidity gap between Y and X, and X is the diffractive mass. Kinematic variables: t — momentum transfer at the proton vertex, ξ — longitudinal momentum fraction of the proton carried by the Pomeron, and β — longitudinal momentum fraction of the Pomeron carried by the parton. Right: Incoherent diffraction on nuclei. The final state A^* can be a nucleus in an excited state which can further disintegrate into another nucleus and any number of nucleons.

comes from gluons, and thus this process offers a unique window to study proton structure, particularly at small x. Diffractive structure functions can be used to pin down the details of the QCD evolution, and in particular the deviation from the linear regime. It has also been demonstrated that diffraction in ep scattering is related to the mechanism of nuclear shadowing. Finally, diffractive DIS allows for the precise extraction of the diffractive PDFs and tests of the limits of collinear factorisation.

Both the LHeC and its higher energy version, the FCC-eh, offer unprecedented capabilities for studying diffraction. The extended kinematic regime in (x, Q^2) of both machines translates into a wider range of available momentum fraction ξ of the diffractive exchange with respect to the hadron, down to $10^{-4} - 10^{-5}$ for a wide range of the momentum fraction of the parton β with respect to the diffractive exchange. See Fig. 5 for the definition of variables. The high luminosity, the extended lever arm both in x and Q^2, and diffractive variables ξ, β for the LHeC and FCC-eh would allow for much tighter constraints of the diffractive parton densities compared to HERA. Furthermore, new possibilities in diffraction open up at these machines. The higher energy allows top quark production to be studied in diffraction, which can be important, particularly at the FCC-eh. Also, charged current diffraction could be measured with much greater precision than at HERA. The dijet diffractive production can be studied in a much greater kinematic range than at HERA and thus impact on the extraction of diffractive PDFS, and the limits of diffractive factorisation could be explored.

Exclusive diffraction opens up new possibilities, particularly for exploring the spatial structure of the hadron at high energy. The diffractive exclusive vector meson production at small x provides information about gluons, and is sensitive to non-linear evolution. The energy dependence of this process can provide information about changes in the dynamics from linear to non-linear. The differential cross section and the t-slope measurements can give insight into small-x dynamics even further. Theoretical calculations show that the differential cross section will have dips, or minima, which occur when the saturated regime is reached. The position of these minima varies with the photon-hadron energy and Q^2 of the virtual photon, thus providing a handle to pin down saturation at small x. Other processes which are valuable sources for the proton structure are Deeply Virtual Compton Scattering, which can provide information about the quark distribution and its spatial extent, as well as the diffraction dissociation for protons which can be useful in the context of studying density fluctuations in the proton.

In the nuclear case, diffraction becomes a more involved process than in *ep* due to the fact that in addition to coherent $e + \mathrm{A} \to e + \mathrm{A} + X$, left plot of Fig. 5 with the replacement $p \to A$, there is also incoherent $e + \mathrm{A} \to e + \mathrm{A}^* + X$ diffraction, where A^* is an excited nuclear state, see the right plot of Fig. 5. The difficulty is to distinguish the two processes or even veto one of them. Additionally, the reconstruction of the diffractive kinematic variables becomes challenging. If such difficulties, which also exist in UPCs at hadronic colliders, are resolved, a wealth of information on nuclei can be obtained using the same observables as in *ep*.[1]

By investigating coherent and incoherent diffractive scattering on nuclei, unique insight into the spatial structure of matter is obtained. On one hand, the coherent cross section, which dominates for $-t \leqslant 1/R_p^2$, is sensitive to the average spatial density distribution of gluons in transverse space. On the other hand, the incoherent cross section, dominant for $-t > 1/R_p^2$, provides information on nuclear dissociation and measures fluctuations of the gluon density inside the nucleus down to subnucleon scales. The t-distribution in coherent diffractive production off the nucleus gives rise to a dip-type structure for both saturation and non-saturation models. Meanwhile, in the case of incoherent production at small $|t|$, neither saturation and non-saturation models lead to dips.[23] This is in drastic contrast to the diffractive production off the proton where only saturation models lead to a dip-type structure in the t-distribution at values of $|t|$ that can be experimentally accessible. Therefore, diffractive production offers a unique opportunity to measure the spatial distribution of partons in the protons and nuclei. It is also an excellent tool to investigate the approach to unitarity in the high energy limit of QCD. Note that diffractive partonic densities inside nuclei are completely unknown, see the recent review[24] and[25] for studies at the LHeC and FCC-he.

Besides its intrinsic interest, spatial information on the partonic structure of nuclei is crucial for the interpretation and precise extraction of the properties of the medium created in small collision systems and in heavy ion collisions, see Ref. 1. While the EIC will produce such information, it does so for values of x larger than those relevant for the LHC and future hadronic colliders. Our present knowledge of parton evolution towards smaller x is largely insufficient for a reliable extrapolation of the findings at the EIC.

3. Small-x dynamics

At the small values of x accessible at very high energy electron-hadron and hadron-hadron collisions, terms containing large logarithms of $\ln 1/x$ appear that need to be included in the formalism. Thus, even at very small values of the strong coupling $\alpha_s \ll 1$, in the perturbative regime, the powers $\alpha_s \ln 1/x \sim 1$ are large and thus need to be resummed. The Balitsky-Fadin-Kuraev-Lipatov (BFKL) evolution equation[26,27] accomplishes that goal and is available at LL and NLL accuracy. It is thus predicted that the parton density evolution will be modified by the small-x effects for collisions performed at sufficiently high energies. The small-x evolution requires matching to the collinear DGLAP evolution, and additional constraints from kinematics are also needed to stabilize the results. Resummation procedures have been developed over the years,[28,29] and allow predictions of the growth of parton densities and structure functions at very small x. Studies using small-x resummation in the collinear approach[30] have demonstrated that the description of the structure functions at HERA at small x is improved compared to that in fixed order DGLAP evolution. In particular, detailed studies have shown that the improvement in the description is greatest for the small-x and small-Q^2 region, exactly where the small-x logarithms are expected to be significant.

This has important consequences for the predictions at higher energies accessible at LHeC. The differences between DGLAP evolution and the evolution based on the small-x resummation are significant at small x for inclusive quantities like F_2 and F_L. The longitudinal structure function F_L is particularly sensitive, and the LHeC (even more so the FCC-eh) can easily distinguish between the different evolution scenarios, see Fig. 6.

In all its realisations, non-linear QCD dynamics leading to saturation[31,32] are density effects, i.e., parton recombination balances splitting when parton densities become large. This happens not only for small values of x, but also when the number of nucleons A increases. Indeed, the squared saturation momentum Q_s^2 that provides the momentum scale below which gluon density is saturated, increases $\propto A^{1/3}$. Therefore, eA collisions are crucial for the discovery of saturation, as they provide an additional enhancement of the perturbative region where saturation effects should be noticeable, $\Lambda^2_{\rm QCD} < Q^2 < Q_s^2$. They are also key in establishing the mechanism of saturation, e.g., the weak coupling one provided by the CGC.[31,32] Finally, nuclear effects should offer the possibility to distinguish between new linear QCD dynamics (resummation of small-x logarithms) — which are not affected by density, and non-linear dynamics.

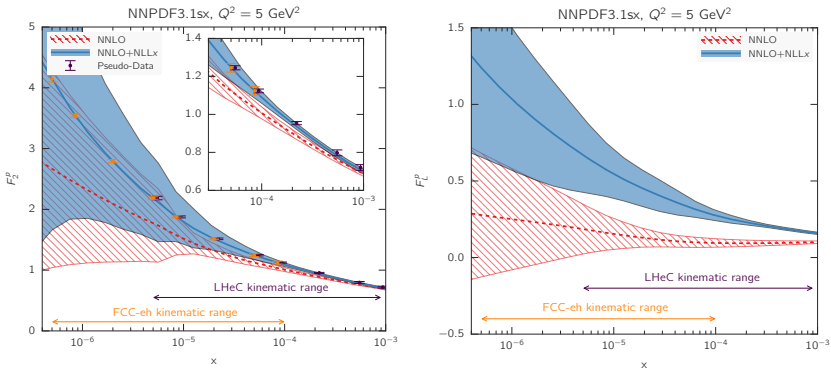

Fig. 6. Predictions for the F_2 and F_L structure functions using the NNPDF3.1sx NNLO and NNLO+NLLx fits at $Q^2 = 5$ GeV^2 for the kinematics of the LHeC and FCC-eh. In the case of F_2, the expected total experimental uncertainties based on the simulated pseudodata are also shown, assuming the NNLO+NLLx values as the central prediction. The LHeC pseudodata have been offset by a small amount for better visibility. The inset in the left plot shows a magnified view in the kinematic region $x > 3 \times 10^{-5}$, corresponding to the reach of HERA data. Figure taken from Ref. 30.

Inclusive observables can be used to search for non-linear effects. Tension appears between the description of F_2 and F_L saturation predictions in models based on DGLAP evolution; see Ref. 33 for a study using reweighting techniques at EIC energies. More recent studies[34] indicate that the difference in Q^2 evolution between linear, DGLAP based models and non-linear models may be a good candidate to observe saturation effects and that the large perturbative lever arm at small x accessible at the LHeC is crucial for this effect to be quantitatively significant. On the other hand, exclusive diffraction shows significant saturation effects as commented in Sec. 2. Other observables like azimuthal correlations among particles at small x are also strongly affected by saturation.[35] Nevertheless, it should be noted that conventional nuclear effects may be hardly distinguishable from weak coupling saturation.[1,36] Therefore, both ep and eA collisions will be required to establish the existence and realisation of non-linear QCD dynamics.

Finally, the dynamics of QCD at small x or large energies will have strong consequences on hadronic and nuclear collisions. It will determine particle production at the initial stage of hadronic collisions. As indicated previously, our lack of knowledge on this matter limits our ability to characterise the medium produced in proton-nucleus and nucleus-nucleus collisions at LHC energies. Therefore, eA collisions at the LHeC become necessary for the full exploitation of the heavy-ion program at the LHC.

References

1. P. Agostini *et al.* [LHeC and FCC-he Study Group], J. Phys. G **48**, no. 11, 110501 (2021) doi:10.1088/1361-6471/abf3ba [arXiv:2007.14491 [hep-ex]].
2. K. D. J. André, L. Aperio Bella, N. Armesto, S. A. Bogacz, D. Britzger, O. S. Brüning, M. D'Onofrio, E. G. Ferreiro, O. Fischer, C. Gwenlan *et al.*, Eur. Phys. J. C **82**, no. 1, 40 (2022) doi:10.1140/epjc/s10052-021-09967-z [arXiv:2201.02436 [hep-ex]].
3. R. Abdul Khalek, A. Accardi, J. Adam, D. Adamiak, W. Akers, M. Albaladejo, A. Al-bataineh, M. G. Alexeev, F. Ameli, P. Antonioli *et al.*, Nucl. Phys. A **1026**, 122447 (2022) doi:10.1016/j.nuclphysa.2022.122447 [arXiv:2103.05419 [physics.ins-det]].
4. H. Abramowicz *et al.* [H1 and ZEUS], Eur. Phys. J. C **75** (2015) no. 12, 580 doi:10.1140/epjc/s10052-015-3710-4 [arXiv:1506.06042 [hep-ex]].
5. R. D. Ball *et al.* [NNPDF], Eur. Phys. J. C **82** (2022) no. 5, 428 doi:10.1140/epjc/s10052-022-10328-7 [arXiv:2109.02653 [hep-ph]].
6. S. Bailey, T. Cridge, L. A. Harland-Lang, A. D. Martin and R. S. Thorne, Eur. Phys. J. C **81** (2021) no. 4, 341 doi:10.1140/epjc/s10052-021-09057-0 [arXiv:2012.04684 [hep-ph]].
7. T. J. Hou, J. Gao, T. J. Hobbs, K. Xie, S. Dulat, M. Guzzi, J. Huston, P. Nadolsky, J. Pumplin, C. Schmidt *et al.*, Phys. Rev. D **103** (2021) no. 1, 014013 doi:10.1103/PhysRevD.103.014013 [arXiv:1912.10053 [hep-ph]].
8. S. Alekhin, J. Bluemlein, S. O. Moch and R. Placakyte, PoS **DIS2016** (2016), 016 doi:10.22323/1.265.0016 [arXiv:1609.03327 [hep-ph]].
9. W. G. Seligman, C. G. Arroyo, L. de Barbaro, P. de Barbaro, A. O. Bazarko, R. H. Bernstein, A. Bodek, T. Bolton, H. S. Budd, J. Conrad *et al.*, Phys. Rev. Lett. **79** (1997), 1213–1216, doi:10.1103/PhysRevLett.79.1213 [arXiv:hep-ex/9701017 [hep-ex]].
10. M. Tzanov *et al.* [NuTeV], Phys. Rev. D **74** (2006), 012008 doi:10.1103/PhysRevD.74.012008 [arXiv:hep-ex/0509010 [hep-ex]].
11. G. Onengut *et al.* [CHORUS], Phys. Lett. B **632** (2006), 65–75 doi:10.1016/j.physletb.2005.10.062
12. J. P. Berge, H. Burkhardt, F. Dydak, R. Hagelberg, M. Krasny, H. J. Meyer, P. Palazzi, F. Ranjard, J. Rothberg, J. Steinberger *et al.*, Z. Phys. C **49** (1991), 187–224 doi:10.1007/BF01555493
13. O. Samoylov *et al.* [NOMAD], Nucl. Phys. B **876** (2013), 339–375 doi:10.1016/j.nuclphysb.2013.08.021 [arXiv:1308.4750 [hep-ex]].
14. G. Aad *et al.* [ATLAS], Phys. Rev. Lett. **109** (2012), 012001 doi:10.1103/PhysRevLett.109.012001 [arXiv:1203.4051 [hep-ex]].
15. S. Chatrchyan *et al.* [CMS], JHEP **02** (2014), 013, doi:10.1007/JHEP02(2014)013 [arXiv:1310.1138 [hep-ex]].
16. G. Aad *et al.* [ATLAS], JHEP **05** (2014), 068 doi:10.1007/JHEP05(2014)068 [arXiv:1402.6263 [hep-ex]].
17. M. Aaboud *et al.* [ATLAS], Eur. Phys. J. C **77** (2017) no. 6, 367 doi:10.1140/epjc/s10052-017-4911-9 [arXiv:1612.03016 [hep-ex]].

18. S. Alekhin, J. Blümlein and S. Moch, Phys. Lett. B **777** (2018), 134–140 doi:10.1016/j.physletb.2017.12.024 [arXiv:1708.01067 [hep-ph]].
19. A. M. Cooper-Sarkar and K. Wichmann, Phys. Rev. D **98** (2018) no. 1, 014027 doi:10.1103/PhysRevD.98.014027 [arXiv:1803.00968 [hep-ex]].
20. S. Alekhin, J. Blümlein, S. Kulagin, S. O. Moch and R. Petti, PoS **DIS2018** (2018), 008 doi:10.22323/1.316.0008 [arXiv:1808.06871 [hep-ph]].
21. V. Andreev *et al.* [H1], Eur. Phys. J. C **74** (2014) 4 doi:10.1140/epjc/s10052-014-2814-6 [arXiv:1312.4821 [hep-ex]].
22. K. J. Eskola, P. Paakkinen, H. Paukkunen and C. A. Salgado, Eur. Phys. J. C **77**, no. 3, 163 (2017) doi:10.1140/epjc/s10052-017-4725-9 [arXiv:1612.05741 [hep-ph]].
23. H. Mäntysaari and B. Schenke, Phys. Lett. B **772**, 832–838 (2017) doi:10.1016/j.physletb.2017.07.063 [arXiv:1703.09256 [hep-ph]].
24. L. Frankfurt, V. Guzey, A. Stasto and M. Strikman, Rept. Prog. Phys. **85** (2022) no. 12, 126301 doi:10.1088/1361-6633/ac8228 [arXiv:2203.12289 [hep-ph]].
25. N. Armesto, P. R. Newman, W. Słomiński and A. M. Staśto, Phys. Rev. D **100**, no. 7, 074022 (2019) doi:10.1103/PhysRevD.100.074022 [arXiv:1901.09076 [hep-ph]].
26. E. A. Kuraev, L. N. Lipatov and V. S. Fadin, Sov. Phys. JETP **45** (1977), 199–204.
27. I. I. Balitsky and L. N. Lipatov, Sov. J. Nucl. Phys. **28** (1978), 822–829.
28. M. Ciafaloni, D. Colferai, G. P. Salam and A. M. Stasto, JHEP **08** (2007), 046 doi:10.1088/1126-6708/2007/08/046 [arXiv:0707.1453 [hep-ph]].
29. G. Altarelli, R. D. Ball and S. Forte, Nucl. Phys. B **799** (2008), 199–240 doi:10.1016/j.nuclphysb.2008.03.003 [arXiv:0802.0032 [hep-ph]].
30. R. D. Ball, V. Bertone, M. Bonvini, S. Marzani, J. Rojo and L. Rottoli, Eur. Phys. J. C **78** (2018) no. 4, 321 doi:10.1140/epjc/s10052-018-5774-4 [arXiv:1710.05935 [hep-ph]].
31. Y. V. Kovchegov and E. Levin, Camb. Monogr. Part. Phys. Nucl. Phys. Cosmol. **33**, 1–350 (2012) doi:10.1017/CBO9781139022187
32. F. Gelis, E. Iancu, J. Jalilian-Marian and R. Venugopalan, Ann. Rev. Nucl. Part. Sci. **60**, 463–489 (2010) doi:10.1146/annurev.nucl.010909.083629 [arXiv:1002.0333 [hep-ph]].
33. C. Marquet, M. R. Moldes and P. Zurita, Phys. Lett. B **772**, 607–614 (2017) doi:10.1016/j.physletb.2017.07.035 [arXiv:1702.00839 [hep-ph]].
34. N. Armesto, T. Lappi, H. Mäntysaari, H. Paukkunen and M. Tevio, Phys. Rev. D **105** (2022) no. 11, 114017 doi:10.1103/PhysRevD.105.114017 [arXiv:2203.05846 [hep-ph]].
35. J. L. Abelleira Fernandez *et al.* [LHeC Study Group], J. Phys. G **39**, 075001 (2012) doi:10.1088/0954-3899/39/7/075001 [arXiv:1206.2913 [physics.acc-ph]].
36. N. Armesto, J. Phys. G **32**, R367–R394 (2006) doi:10.1088/0954-3899/32/11/R01 [arXiv:hep-ph/0604108 [hep-ph]].